Polyhedron 30 (2011) 851–859

Contents lists available at ScienceDirect

Polyhedron

journal homepage: www.elsevier.com/locate/poly

Integrated X-ray crystallography, optical and computational methods in studies of structure and luminescence of new synthesized complexes of lanthanides with ligands derived from 2,6-diformylpyridine

Gelson Manzoni de Oliveira [a,*], Aline Machado [a], Geraldo Wachholz Gomes [a], Jorge H.S.K. Monteiro [b], Marian R. Davolos [b], Ulrich Abram [c], Alexander Jagst [c]

[a] Universidade Federal de Santa Maria, UFSM, Departamento de Química, 97105-900 Santa Maria, RS, Brazil
[b] Universidade Estadual Paulista, UNESP, Instituto de Química, Laboratório de Materiais Luminescentes, Rua Francisco Degni s/n, 14800-900 Araraquara, SP, Brazil
[c] Freie Universität Berlin, Institute of Chemistry and Biochemistry, Fabeckstr. 34-36, D-14195 Berlin, Germany

ARTICLE INFO

Article history:
Received 21 October 2010
Accepted 16 December 2010
Available online 21 December 2010

Keywords:
Lanthanides chelate complexes
Luminescence
Europium(III) luminescent complexes

ABSTRACT

The reaction of 2,6-diformylpyridine-bis(benzoylhydrazone) [dfpbbh] and 2,6-diformylpyridine-bis (4-phenylsemicarbazone) [dfpbpsc] with lanthanides salts yielded the new chelates complexes $[Eu(dfpbpsc-H^+)_2]NO_3$ (**1**), $[Dy(fbhmp)_2][Dy(dfpbbh-2H^+)_2]\cdot 2EtOH\cdot 2H_2O$ (fbhmp = 2-formylbenzoylhydrazone-6-methoxide-pyridine; Ph = phenyl; Py = pyridine; Et = ethyl) and $[Er_2(dfpbbh-2H^+)_2(\mu\text{-}NO_3)(H_2O)_2(OH)]\cdot H_2O$.

X-ray diffraction analysis was employed for the structural characterization of the three chelate complexes. In the case of complex **1**, optical, synthetic and computational methods were also exploited for ground state structure determinations and triplet energy level of the ligand and HOMO–LUMO calculations, as well as for a detailed study of its luminescence properties.

1. Introduction

Reactions of lanthanides with polydentate oxygen and nitrogen ligands have attracted great interest because of the ability of these (hard base) sites to realize stable chelate complexes with high coordination numbers. Moreover, many of these ligands are quite efficient with regards to the displacement of the water molecules which usually are present in the coordination sphere of the lanthanide ions. As is known, the vibrational levels of the O–H bonds of the water lead to the quenching of the luminescence – in the case of luminescent lanthanides ions – by absorption of the emitted radiation in the vibrational excitation processes [1]. In addition, we have already shown that some polydentate nitrogen ligands are able to transfer energy to a lanthanide ion, thus exciting its luminescence – the so-called "antenna" effect [2–4]. Although relatively recent, the chemistry of lanthanides and actinides ions with ligands derived from 2,6-diformylpyridine and 2,6-diacetylpyridine is fairly reach and interesting. Besides previous work in this area, directed to the synthesis and structural properties and performed by Cundari [5] and Gaye [6], in 2005 were reported [7] the synthesis and the crystallographic characterization of four compounds of this kind, among them the complex cation bis(2,6-diformylpyridine-4-phenylsemicarbazone-4-phenylthiosemicarbazonato)samarium(III), the first lanthanide complex in which a thiosemicarbazide appears as ligand. A new series of lanthanides chelate complexes with these ligand types was newly further described by the same group [8], covering and extensive range of metal ions and structures. The research interests, however, were chiefly pointed toward achievable properties of the compounds that would enable their applications in the nuclear medicine.

The polydentate ligands derived from 2,6-diformylpyridine and 2,6-diacetylpyridine are mostly symmetric and good chelating agents for lanthanide ions, but so far they have not been outstanding by their fluorescent activities, still less by their ability to transfer energy to a lanthanide ion and so excite its luminescence. In this work we attempt to enlarge the performance of this kind of compounds, by exploiting the optical properties of novel, uncommon structures.

The lanthanides are characterized by the electronic configuration [Xe] $4f^n$, and their most common oxidation state is 3^+. The $4f^n$ electrons are shielded by the outer lying $5s^25p^6$ subshells. This shielding leads to a low influence of ligand field effects and promotes few changes in the emission spectrum of the ion, in comparison with its atomic spectrum. The energy gaps between electronic states generated by $4f^n$ electrons can range from UV up to near infrared, depending on the element (Gd^{3+}: UV transitions; Sm^{3+}: orange; Eu^{3+}: red; Tb^{3+}: green; Tm^{3+}: blue; Nd^{3+}: near infrared) [9]. The Eu^{3+} ion is one of the most explored due to the easy interpretation of its transitions and the great number of informa-

* Corersponding author. Tel.: +55 55 3220 8757; fax: +55 55 3220 8031.
E-mail address: manzonideo@smail.ufsm.br (G.M. de Oliveira).

0277-5387/$ - see front matter © 2010 Elsevier Ltd. All rights reserved.
doi:10.1016/j.poly.2010.12.021

tion that can be acquired from its luminescence studies. Because of that, the Eu^{3+} ion can be used as structural probes [10], in immunobiological assays [11] and electroluminescent devices [12,13]. In 1990 the use of theoretical methods based upon luminescence experiments was started to predict the ground state geometry, as well as the coordination polyhedron of lanthanide compounds [14], in special Eu^{3+} complexes.

We report now some further results on the complex structural chemistry of lanthanides and ligands derived from 2,6-diformylpyridine, together with luminescence studies carried out with the new chelates $[Eu(dfpbpsc–H^+)_2]NO_3$ (**1**) (dfpbpsc = 2,6-diformylpyridine-bis(4-phenylsemicarbazone), $[Dy(fbhmp)_2][Dy(dfpbbh–2H^+)_2]\cdot 2EtOH\cdot 2H_2O$ (**2**) (fbhmp = 2-formylbenzoylhydrazone-6-methoxide-pyridine; Ph = phenyl; Py = pyridine; Et = ethyl; dfpbbh = 2,6-diformylpyridine-bis(benzoylhydrazone), and $[Er_2(dfpbbh–2H^+)_2(\mu\text{-}NO_3)(H_2O)_2(OH)]\cdot H_2O$ (**3**).

We demonstrate also the worth of the theoretical methods associated with the characteristic transitions of the Eu^{3+} luminescence in corroborating the structural results obtained by X-ray crystallography and other spectroscopic methods.

2. Experimental

The single ligands dfpbbh and dfpbpsc were analyzed mainly through IR spectroscopy. The metal centers of the complexes **1**, **2** and **3** were confirmed through EDX spectra and the monocrystals of the products were evaluated also through Scanning Electron Microscopy. The reference complex cation of gadolinium $[Gd(dfpbpsc–H^+)_2]^+$ (see Section 3.4), analogous to complex $[Eu(dfpbpsc–H^+)_2]NO_3$ (**1**), was synthesized according to the experimental procedures for the preparation of **1** and was also structurally characterized through X-ray crystallography. Since the cell parameters and further crystallographic data of the gadolinium(III) complex are basically the same that those of complex **1**, they were not included in Table 1. The structural formulae of the ligands 2,6-diformylpyridine-bis(benzoylhydrazone), dfpbbh, and 2,6-diformylpyridine-bis(4-phenylsemicarbazone), dfpbpsc, are given in Chart A. Both ligands were prepared starting from 2,6-diformylpyridine, according to literature procedures [8].

Table 1
Crystallographic data and refinement parameters for **1**, **2** and **3**.

Empirical formula	$C_{42}H_{36}EuN_{16}O_{10}$	$C_{74}H_{70}Dy_2N_{16}O_{12}$	$C_{42}H_{37}Er_2N_{11}O_{11}$
Formula weight	1076.82	1700.46	1206.35
T (K)	293(2)	293(2)	293(2)
Crystal system	monoclinic	triclinic	monoclinic
Space group	$C2/c$	$P\bar{1}$	$C2/c$
a (Å)	16.0374(12)	14.0350(16)	19.4227(4)
b (Å)	19.6982(15)	14.1008(15)	22.1529(4)
c (Å)	19.4788(14)	20.331(2)	25.1724(5)
α (°)	90	70.199(6)	90
β (°)	99.935(3)	70.483(5)	91.906(2)
γ (°)	90	82.925(6)	90
V (Å^3)	6061.2(8)	3568.0(7)	10824.9(4)
Z	4	2	8
ρ_{calc} (g cm^{-3})	1.180	1.583	1.480
μ (Mo Kα) (mm^{-1})	1.092	2.152	3.139
λ (Å)	0.71073	0.71073	0.71073
F (0 0 0)	2172	1708	4720
Collected reflections	39987	53289	86082
Unique reflections	4691	15864	11591
Goodness-of-fit (F^2)	1.147	1.130	0.995
R_1[a]	0.0673	0.0273	0.0538
wR_2[b]	0.2307	0.0891	0.1895

[a] $R_1 = \Sigma||F_o| - |F_c||/\Sigma|F_o|$.
[b] $wR_2 = \{\Sigma w(F_o^2 - F_c^2)^2/\Sigma w(F_o^2)^2\}^{1/2}$.

2.1. Preparation of $[Eu(dfpbpsc–H^+)_2]NO_3$ (**1**)

To a suspension of 0.0401 g (0.1 mmol) of dfpbpsc in 10 mL of ethanol, a solution of 0.0214 g (0.05 mmol) of $Eu(NO_3)_3\cdot 5H_2O$ in 5 mL of ethanol was added. After addition of three drops of triethylamine the suspension was refluxed by 3 h. The red mixture was then cleaned by filtration. The slow evaporation of the solvent led to the formation of yellow crystals. Yield: 53% based on $Eu(NO_3)_3\cdot 5H_2O$.

Properties: yellow crystalline substance. Melting point: 276 °C. *Anal.* Calc. for $C_{42}H_{36}EuN_{16}O_{10}$ (1076.82): C, 49.69; H, 7.42; N, 14.74. Found: C, 49.71; H, 7.58; N, 14.85%. IR (KBr): 3384.2 [ν_s(N–H), strong], 1597.1 [ν_s(C=C), medium], 1693.2 [ν_s(C=O), strong], 1237.6 [ν_s(N=C), medium], 1163.6 cm^{-1} [ν_s(N–N), medium].

2.2. Preparation of $[Dy(fbhmp)_2][Dy(dfpbbh–2H^+)_2]\cdot 2EtOH\cdot 2H_2O$ (**2**)

A solution of 0.01878 g (0.05 mmol) of hydrated dysprosium(III) chloride with 99.9% purity (purchased by Sigma–Aldrich), in 5 mL of ethanol, was added to a suspension prepared by partial dissolution of 0.0371 g (0.1 mmol) of dfpbbh in 10 mL of ethanol. After addition of three drops of triethylamine the suspension was refluxed by 3 h and then filtered. A layer of *n*-hexane was added over the filtrate, and its slow evaporation yielded orange yellow crystals of **2**. Yield: 36% based on the Dy salt.

Properties: orange yellow crystalline compound. Melting point: 275 °C. *Anal.* Calc. for $C_{74}H_{70}Dy_2N_{16}O_{12}$ (1700.46): C, 52.00; H, 5.87; N, 13.28. Found: C, 51.73; H, 6.06; N, 13.12%. IR (KBr): 3338.0 [ν_s(N–H), s], 1586.5 [ν_s(C=C), m], 1640.8 [ν_s(C=O), s], 1293.2 [ν_s(N=C), m], 1147.2 cm^{-1} [ν_s(N–N), m].

2.3. Preparation of $[Er_2(dfpbbh–2H^+)_2(\mu\text{-}NO_3)(H_2O)_2(OH)]\cdot H_2O$ (**3**)

0.0190 g (0.05 mmol) of hydrated erbium(III) chloride with 99.9% purity (purchased by Sigma–Aldrich) plus 0.0371 g (0.1 mmol) of dfpbbh were dissolved in 15 mL of ethanol. After addition of three drops of triethylamine the suspension was refluxed by 3 h and then filtered. The slow evaporation of the greenish yellow mother solution yielded yellow crystals of the product. Yield: 42% based on the Er salt.

Properties: yellow crystalline substance. Melting point: 266 °C. *Anal.* Calc. for $C_{42}H_{37}Er_2N_{11}O_{11}$ (1206.35): C, 50.50; H, 5.28; N, 12.96. Found: C, 50.52; H, 5.87; N, 12.92%. IR (KBr): 3396.4 [ν_s(N–H), s], 1577.9 [ν_s(C=C), m], 1660.7 [ν_s(C=O), s], 1273.0 [ν_s(N=C), m], 1148.3 cm^{-1} [ν_s(N–N), m].

2.4. X-ray structural determination

Data were collected with a Bruker APEX II CCD area-detector diffractometer and graphite-monochromatized Mo Kα radiation. The crystal structures were solved by direct methods using SHELXS [15]. Subsequent Fourier-difference map analyses yielded the positions of the non-hydrogen atoms. Refinements were carried out with SHELXL package [15]. All refinements were made by full-matrix least-squares on F^2 with anisotropic displacement parameters for all non-hydrogen atoms. Hydrogen atoms were included in the refinement in calculated positions.

2.5. Optical and luminescence experiments

The electronic absorption spectrum of the ligands was performed in dimethyl sulfoxide (DMSO) solutions in a Perkin–Elmer Lambda 14P spectrophotometer in the range between 200 and 500 nm. The excitation and emission spectra were performed at ~77 K in a Horiba Jobin Yvon model FL3-222 equipped with a

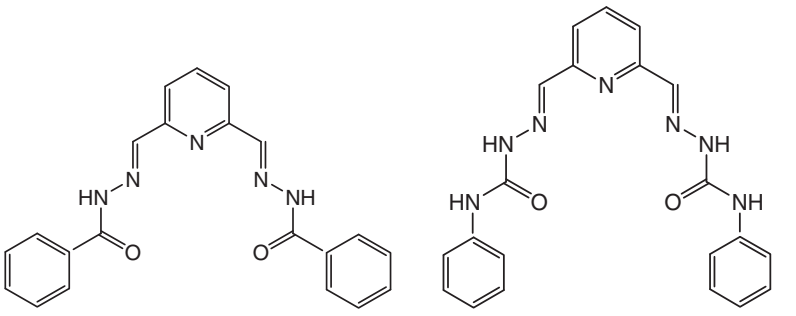

Chart 1.

450W continuum Xenon Lamp. The emission lifetime of the $^5D_0$ state was performed using a Jobin Yvon phosphorimeter model FL1040 and pulse lamp; we used 329 nm as excitation wavelength and 612 nm as emission wavelength.

The semi empirical method with basis on luminescence studies has advantages due the low computer time for calcules and high accuracy in the prediction of bond lengths and bond angles. The Sparkle/AM1 methodology [16] was developed and implemented in the MOPAC2009 package [17] (recent results [18–20] show good agreements when compared to monocrystal data from the ground state geometry). Using the INDO/S-CIS (Intermediate Neglect Differential Overlap/Spectroscopy – Configuration Interaction Simple) [21,22], implemented in ZINDO package [23] and the data generated by Sparkle/AM1, it is possible to calculate the singlet and triplet levels of the organic ligand in the complex.

3. Results and discussion

3.1. Crystal structure

The X-ray crystal data and the experimental conditions for the analyses of $[Eu(dfpbpsc–H^+)_2]NO_3$ (**1**), $[Dy(fbhmp)_2][Dy(dfpbbh–2H^+)_2]\cdot 2EtOH\cdot 2H_2O$ (**2**) and $[Er_2(dfpbbh–2H^+)_2(\mu\text{-}NO_3)(H_2O)_2(OH)]\cdot H_2O$ (**3**) are given in Table 1. Fig. 1 shows the molecular structure of **1**, with exception of the NO_3 (counter) ion. Figs. 2 and 3 display the cationic and anionic components of complex **2**, respectively $[Dy(fbhmp)_2]^+$ and $[Dy(dfpbbh–2H^+)_2]$, without showing the solvate molecules (ethanol and water), for clarity. Fig. 4 depicts the structure of the binuclear complex **3**, also without the solvate molecule. All the significant bond lengths and angles of the title complexes were included in the figure captions. Lanthanides(III) are known for their ability to perform chelate complexes with high coordination numbers. The metal center in the europium complex **1** presents coordination number 10, and its coordination polyhedron is clearly a bicapped cube, or elongated square dipyramid (see Section 3.4). In the anionic component of complex **2**, $[Dy(dfpbbh–2H^+)_2]^-$, also the dysprosium ion attains the coordination number 10, with a biccapped cube as coordination polyhedron (Fig. 3). The dysprosium center of the cationic complex $[Dy(fbhmp)_2]^+$ (**2**) (Fig. 2) presents, however, coordination number 8, forming a distorted cube. In the binuclear complex $[Er_2(dfpbbh–2H^+)_2(\mu\text{-}NO_3)(H_2O)_2(OH)]\cdot H_2O$ (**3**) the metal centers present different coordination numbers: Er1 shows coordination number 9, and disregarding the bonds Er1–O6 and Er1–O7 (both O6 and O7 from the NO_3^- bridge-forming ligand anion), the seven remaining bonds to Er1 achieve a distorted pentagonal-bipyramidal geometry. Er2, differently, reaches the coordination number 10, and only the bonds Er2–N11, Er2–O5 and Er–O7 (nitrate ion bridge) are in the same plane and close to each other. As a whole, together with the remaining seven Er2 bonds, these three bonds do not attain any coordination polyhedron described in the literature for the coordination number 10 [24].

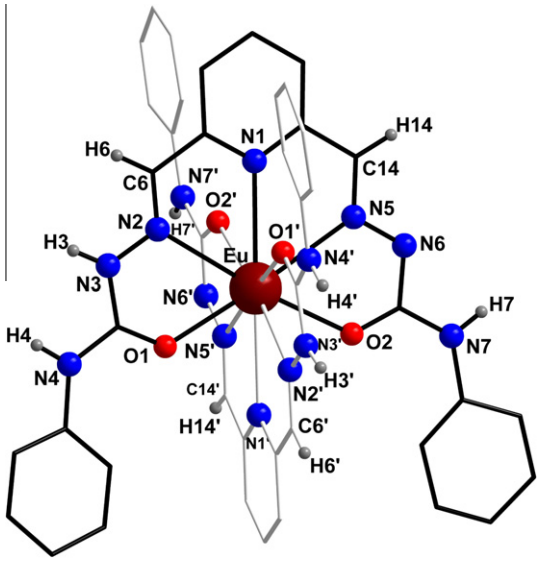

Fig. 1. Molecular structure of $[Eu(dfpbpsc–H^+)_2]NO_3$ (**1**). The hydrogen atoms of the phenyl groups, as well as the solvate NO_3 ion, have been omitted by clarity. Symmetry code: (′) *x*, *y*, *z* + 1.5. Selected bond lengths [Å] and angles [°]: Eu–O1′ 2.408(6), Eu–O1 2.408(6), Eu–O2′ 2.443(6), Eu–O2 2.443(6), Eu–N2′ 2.667(7), Eu–N2 2.667(7), Eu–N5 2.688(7), Eu–N5′ 2.688(7), Eu–N1 2.786(7), Eu–N1′ 2.786(7); O1′–Eu–O1 97.5(3), O1′–Eu–O2′ 124.65(19), O1–Eu–O2′ 103.0(2), O1′–Eu–O2 103.0(2), O1–Eu–O2 124.65(19), O2′–Eu–O2 106.0(3), N2′–Eu–N2 106.1(3), N2′–Eu–N5 108.3(2), N2–Eu–N5 115.8(2), N2′–Eu–N5′ 115.8(2), N2–Eu–N5′ 108.3(2), N5–Eu–N5′ 102.8(3), N2′–Eu–N1 123.8(2), N2–Eu–N1 57.8(2), N5–Eu–N1 58.1(2), N5′–Eu–N1 120.4(2), N2′–Eu–N1′ 57.8(2), N2–Eu–N1′ 123.8(2), N5–Eu–N1′ 120.4(2), N5′–Eu–N1′ 58.1(2), N1–Eu–N1′ 177.9(3).

3.2. Synthesis

In the synthesis of $[Dy(fbhmp)_2][Dy(dfpbbh–2H^+)_2]\cdot 2EtOH\cdot 2H_2O$ (**2**) has occurred partial decomposition of the ligand dfpbbh, resulting the ligand fbhmp. Because of the presence of triethylamine in the reaction enviroment, as well as the occurrence of an hydroxide ion and a water molecule as ligands in complex **3** (Er2 and Er1, respectively, see Fig. 4), it is reasonable to assume that the formation of the ligands fbhmp – giving rise to the cation $[Dy(fbhmp)_2]^+$ – has occurred due to the attack of a OH^- ion to the (pyridine vicinal) HC=N bond of a molecule of dfpbbh, with final formation of the group $–CH_2–O^-$ and further coordination to Dy(III) (C49 and C63, see Fig. 2). This probable secondary reaction is shown in Scheme 1.

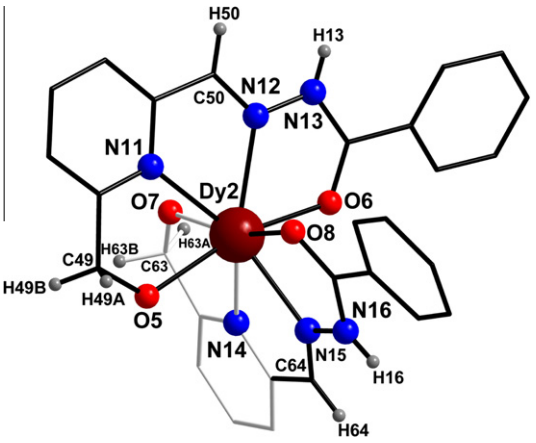

Fig. 2. Structure of the cation $[Dy(fbhmp)_2]^+$ (**2**). The hydrogen atoms of the phenyl groups, as well as the solvates molecules (2EtOH + $2H_2O$) are not shown. Selected bond lengths [Å] and angles [°]: Dy2–O6 2.276(2), Dy2–O8 2.312(2), Dy2–O7 2.357(2), Dy2–O5 2.400(2), Dy2–N12 2.447(3), Dy2–N15 2.462(3), Dy2–N14 2.475(3), Dy2–N11 2.480(3); O6–Dy2–O8 90.17(9), O6–Dy2–O7 92.30(8), O8–Dy2–O7 165.53(8), O6–Dy2–O5 165.19(8), O8–Dy2–O5 93.42(8), O7–Dy2–O5 87.80(8), N12–Dy2–N15 133.87(9), N12–Dy2–N14 133.53(9), N15–Dy2–N14 64.59(9), N12–Dy2–N11 64.77(9), N15–Dy2–N11 140.58(9), N14–Dy2–N11 133.99(9).

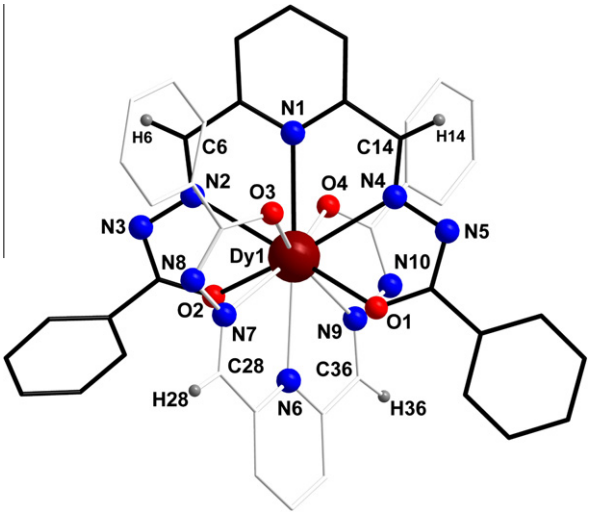

Fig. 3. Structure of the anion $[Dy(dfpbbh–2H^+)_2]$ (**2**). For clarity, the hydrogen atoms of the phenyl groups, as well as the solvates molecules (2EtOH + $2H_2O$), have been omited. Selected bond lengths [Å] and angles [°]: Dy1–O4 2.344(2), Dy1–O1 2.391(2), Dy1–O2 2.429(2), Dy1–O3 2.458(2), Dy1–N7 2.590(3), Dy1–N2 2.591(3), Dy1–N9 2.594(3), Dy1–N4 2.613(3), Dy1–N1 2.701(3), Dy1–N6 2.702(3); O4–Dy1–O1 111.61(8), O4–Dy1–O2 84.49(8), O1–Dy1–O2 130.82(8), O4–Dy1–O3 128.83(8), O1–Dy1–O3 84.23(8), O2–Dy1–O3 122.31(8), N7–Dy1–N2 79.73(9), N7–Dy1–N9 119.07(9), N2–Dy1–N9 128.91(9), N7–Dy1–N4 126.43(9), N2–Dy1–N4 119.01(9), N9–Dy1–N4 88.80(9), N7–Dy1–N1 115.34(9), N2–Dy1–N1 59.45(8), N9–Dy1–N1 125.56(8), N4–Dy1–N1 59.58(8), N7–Dy1–N6 59.49(9), N2–Dy1–N6 118.25(8), N9–Dy1–N6 59.63(9), N4–Dy1–N6 122.35(9), N1–Dy1–N6 174.80(8).

Finally, it must be pointed out, that the occurrence of binuclear chelate complexes of lanthanides ions such as $[Er_2(dfpbbh–2H^+)_2(\mu\text{-}NO_3)(H_2O)_2(OH)]\cdot H_2O$ (**3**) is not common in the literature. The Er1–Er2 distance (4.7642 Å) is remarkable longer than the sum of the Er/Er van der Waals radii (4 Å), and the approximation of both atoms has only occurred because of the rare ability of the trigonal planar NO_3^- ion to perform such a strengthened bridge, engaging its four atoms in the double linkage.

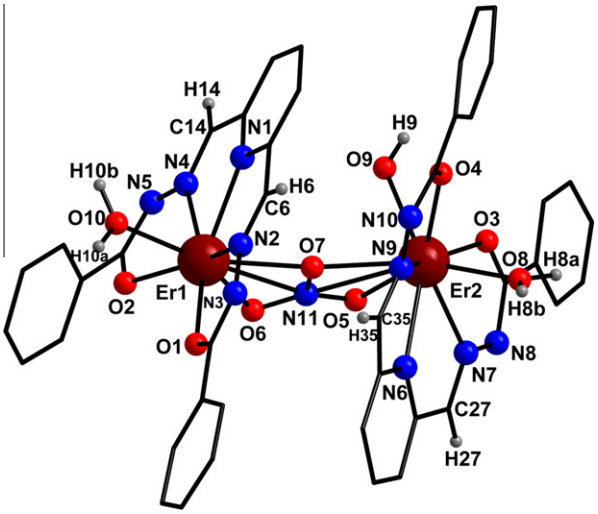

Fig. 4. Molecular structure of $[Er_2(dfpbbh–2H^+)_2(\mu\text{-}NO_3)(H_2O)_2OH]\cdot H_2O$ (**3**). The hydrogen atoms of the phenyl groups, as well as the solvate molecule (H_2O), have been omited for clarity. Selected bond lengths [Å] and angles [°]: Er1–O1 2.263(7), Er1–O2 2.295(7), Er1–O6 2.332(7), Er1–O10 2.346(7), Er1–O7 2.360(6), Er1–N1 2.427(8), Er1–N4 2.435(8), Er1–N2 2.434(8), Er1–N11 2.731(11), Er2–O3 2.330(7), Er2–O8 2.332(7), Er2–O4 2.352(7), Er2–O5 2.393(8), Er2–O7 2.412(6), Er2–O9 2.425(7), Er2–N7 2.515(8), Er2–N6 2.516(8), Er2–N9 2.539(8), Er2–N11 2.818(11); O1–Er1–O2 98.8(2), O1–Er1–O6 96.5(3), O2–Er1–O6 75.6(3), O1–Er1–O10 85.8(3), O2–Er1–O10 78.0(3), O6–Er1–O10 153.5(3), O1–Er1–O7 94.4(3), O2–Er1–O7 131.1(2), O6–Er1–O7 56.2(2), O10–Er1–O7 150.2(2), N1–Er1–N4 64.7(3), N1–Er1–N2 65.0(3), N4–Er1–N2 129.1(3), N1–Er1–N11 94.0(3), N4–Er1–N11 86.1(3), N2–Er1–N11 105.1(3), O3–Er2–O8 81.1(3), O3–Er2–O4 101.2(3), O8–Er2–O4 75.5(3), O3–Er2–O5 82.4(3), O8–Er2–O5 142.4(2), O4–Er2–O5 141.1(3), O3–Er2–O7 130.6(3), O8–Er2–O7 147.9(2), O4–Er2–O7 99.2(2), O5–Er2–O7 54.7(2), O3–Er2–O9 73.1(3), O8–Er2–O9 128.7(3), O4–Er2–O9 67.4(3), O5–Er2–O9 77.0(3), O7–Er2–O9 74.2(3), N7–Er2–N6 62.8(3), N7–Er2–N9 121.3(3), N6–Er2–N9 62.6(3), N7–Er2–N11 87.3(3), N6–Er2–N11 76.9(3), N9–Er2–N11 99.8(3), Er1–N11–Er2 118.3(4), Er1–O7–Er2 173.3(3).

3.3. Optical investigations

Since the Dy (**2**) and Er (**3**) complexes showed no luminescent properties, the main scope of this work regarding optical occurrences is the investigation of the spectroscopic parameters of the europium complex, by calculating the ground state geometry using the Sparkle/AM1 method, as well as the intensity parameters, transfer and back transfer rates and energy levels populations. These results allow to compare the theoretical data with the experimental ones and to use the theoretical data to explain some experimental events.

3.4. Optical features, HOMO–LUMO calculations

The electronic absorption spectrum of the ligand dfpbpsc is depicted in Fig. 5 and shows a broad band due to the $n \rightarrow \pi^*$ transitions of the R–N=N–R groups [25]. It is not possible to obtain the absorption bands below 250 nm because of the cutoff region of the solvent (DMSO). The HOMO and LUMO of the coordinated ligand dfpbpsc–H^+ are shown in Fig. 6 and were calculated according to the RM1 [26] procedures implemented in MOPAC2009 package [17]. The energy gap ranges from −4.2 to 1.9 eV and the HOMO are localized manly in the deprotonated side of the ligand, embracing the C=N–N^-–C=O atoms/bonds, whereas the LUMO are located on the carbonyl group and on the terminal phenyl rest of the protonated ligand side. The HOMO–LUMO energy diagram also shows clearly the deprotonation of the nitrogen atoms N6 and N6′ of the two ligand molecules of the complex $[Eu(dfpbpsc–H^+)_2]NO_3$ (**1**) (see Fig. 1).

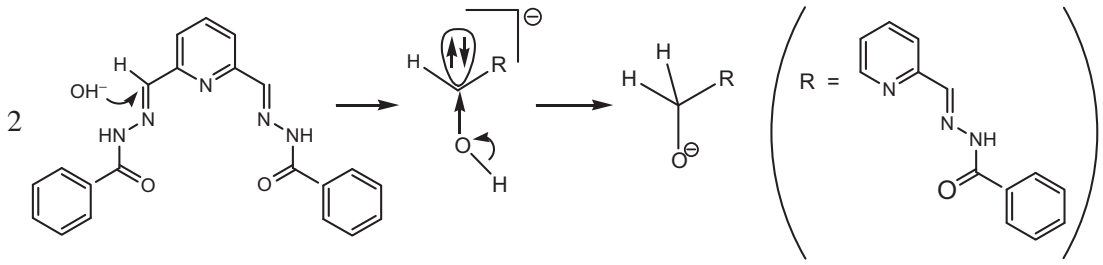

Scheme 1. Mechanism of decomposition of the ligand dfpbbh.

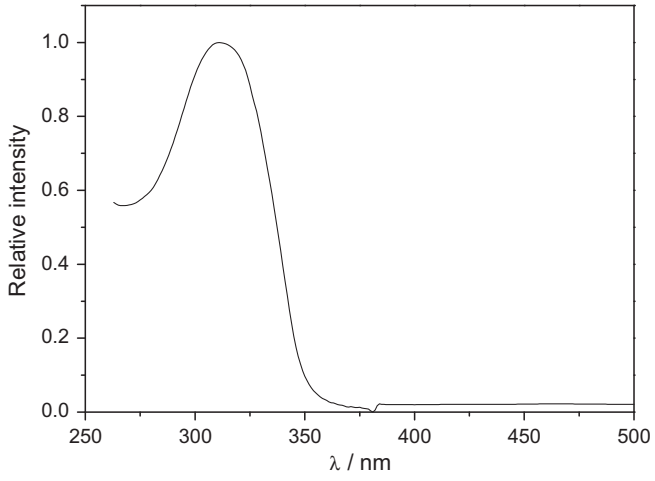

Fig. 5. Electronic absorption spectrum of the ligand dfpbpsc.

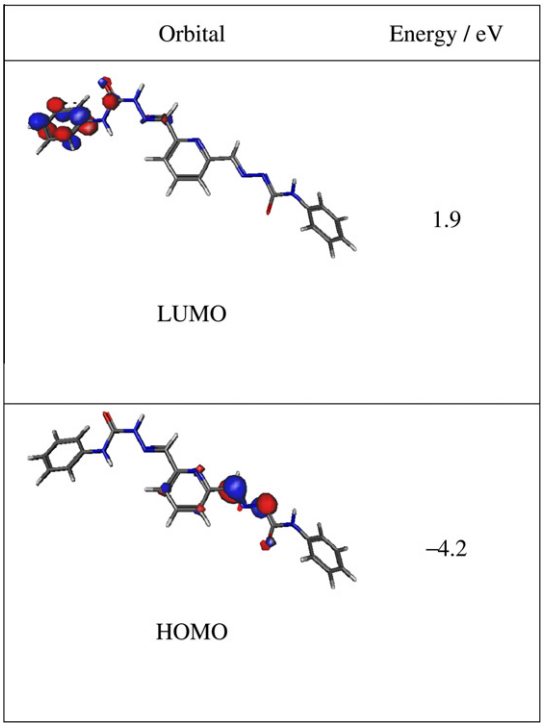

Fig. 6. HOMO and LUMO of the coordinated ligand dfpbpsc–H^+.

3.5. Luminescence spectroscopy and ground state structures

The excitation spectrum of [Eu(dfpbpsc–H^+)$_2$]NO_3 (**1**) is displayed in Fig. 7 and shows a broad band at 329 nm, due to the $S_0 \rightarrow S_1$ transition of the ligand, and narrow bands (396 and 464 nm) as a result of the $^7F_0 \rightarrow {}^5D_2$ and $^7F_0 \rightarrow {}^5L_6$ intraconfigurational transitions of the europium ion. The presence of a broad band in the excitation spectrum is an indicative that there is energy transfer between ligands and the europium ion.

The emission spectrum of **1**, depicted in Fig. 8, shows the characteristic transitions of the europium ion, $^5D_0 \rightarrow {}^7F_J$; $J = 0, 1, 2, 3$ and 4. The transition $^5D_0 \rightarrow {}^7F_2$ appears with the highest intensity in the spectrum, and the high intensity of the $^5D_0 \rightarrow {}^7F_4$ transition can be an indicative of high symmetry around the europium ion [27], as well as a long range effect. The inset of Fig. 8 shows the $^5D_0 \rightarrow {}^7F_0$ transition. The number of $^5D_0 \rightarrow {}^7F_0$ lines is equal to the number of different non centrosymmetric sites around the metal center, and the absence of this transition should be an indicative that the europium ion would lie in a symmetric site. There is at least one line for this transition for complex **1**, therefore the europium ion lies in a non centrosymmetric site.

The analogous complex of gadolinium was synthesized (according to the experimental procedures for the preparation of **1**), to determine the triplet energy level of the ligand. The process is based upon the exceptionally high energy of the lowest excited level of Gd(III), which affords an efficient method for this kind of measurement, after preparing the Gd(III) complex with the compound whose triplet energy is to be measured. The triplet energy is achieved through the centroid of the most intense transition of the emission spectrum, and for the coordinated ligand dfpbpsc–H^+ the triplet energy is located in 23115 cm^{-1}. The emission

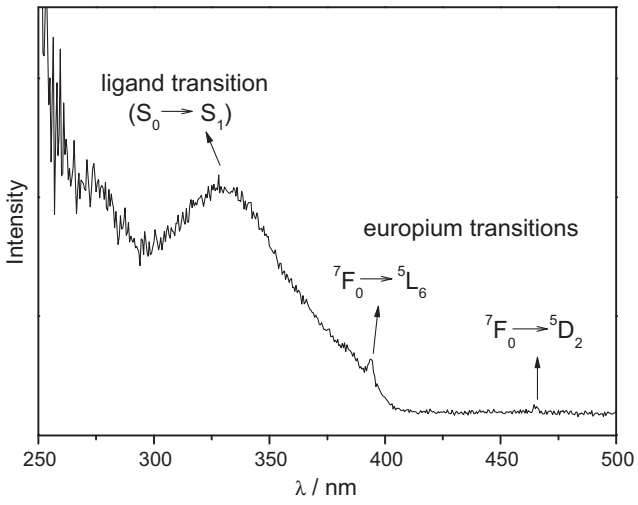

Fig. 7. Excitation spectrum of [Eu(dfpbpsc–H^+)$_2$]NO_3 (**1**), with $\lambda_{em} = 612$ nm at ~298 K.

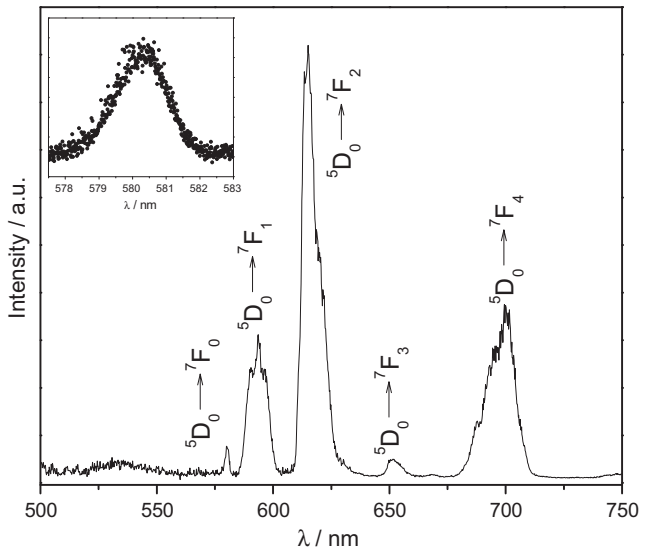

Fig. 8. Emission spectrum of [Eu(dfpbpsc–H^+)$_2$]NO_3 (**1**), with λ_{ex} = 329 nm at ~77 K. The inserted signal amplification covers the range 577.5–583 nm and shows the $^5D_0 \rightarrow {}^7F_0$ transition.

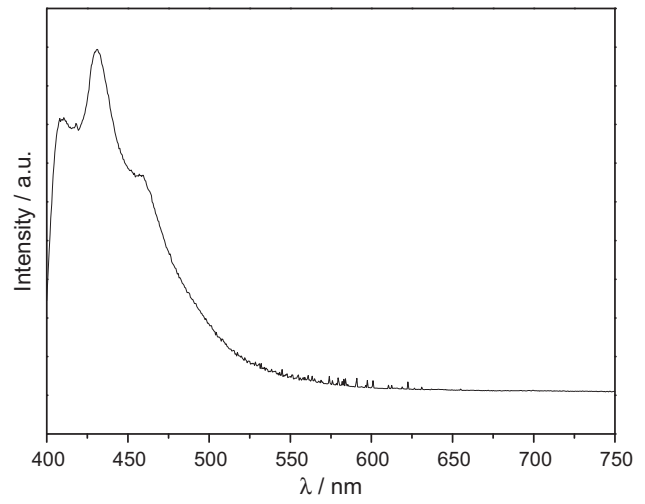

Fig. 9. Emission spectrum of [Gd(dfpbpsc–H^+)$_2$]NO_3, with λ_{ex} = 320 nm at ~77 K.

spectrum of the complex [Gd(dfpbpsc–H^+)$_2$]NO_3 was obtained at ~77 K and is shown in Fig. 9.

From the emission spectra it is also possible calculate the intensity parameters (Ω_2 and Ω_4) with the Eqs. (1) and (2) [28].

$$A_{0J} = A_{01}\left(\frac{I_{0J}}{I_{01}}\right)\cdot\left(\frac{\sigma_{01}}{\sigma_{0J}}\right) \quad (1)$$

where A_{01} = 50 s^{-1}; I_{0J} corresponds to the intensity of the transition $^5D_0 \rightarrow {}^7F_J$ (J = 2, 4); I_{01} corresponds to the intensity of transition $^5D_0 \rightarrow {}^7F_1$; σ_{0J} corresponds to the baricenter of the transition $^5D_0 \rightarrow {}^7F_J$ (J = 2, 4), and σ_{01} corresponds to the baricenter of the transition $^5D_0 \rightarrow {}^7F_1$. With the A_{0J} values it is possible to calculate the intensity parameters according to Eq. (2).

$$\Omega_J = \frac{3\cdot\hbar\cdot c^3\cdot A_{0J}}{4\cdot e^2\cdot\omega^3\cdot\chi\langle{}^7F_J||U^{(J)}||{}^5D_0\rangle^2} \quad (2)$$

where χ is the Lorentz local field correction given by $\chi = n\cdot(n^2+2)\cdot\frac{n^2+2}{9}$, with the refraction index n = 1.5 and $\langle{}^7F_J||U^{(J)}||{}^59m_0\rangle$ whose values are 0.0032 and 0.0023 to J = 2 and J = 4, respectively [28].

The parameter R_{02} was calculated using the Eq. (3).

$$R_{02} = \frac{I_{00}}{I_{02}} \quad (3)$$

where I_{02} and I_{00} are the integrated areas of the transitions $^5D_0 \rightarrow {}^7F_2$ and $^5D_0 \rightarrow {}^7F_0$. The emission lifetime of $^5D_0$ level (τ) allows determining the non-radiative emission rate (A_{nrad}) according to the relation showed below:

$$A_{tot} = \frac{1}{\tau} = A_{rad} + A_{nrad}$$

The quantum efficiency (η) is calculated by the relation:

$$\eta = \frac{A_{rad}}{A_{rad}+A_{nrad}}$$

All these quantities (Ω_2, Ω_4, R_{02}, A_{rad}, A_{nrad}, A_{tot}, τ and η) are shown in Table 2 for complex **1**. The complex shows a very low value of Ω_2 and a high value of Ω_4. The parameter Ω_2 indicates the degree of covalence between ligand and metal and is associated with the local symmetry. The low value of Ω_2 in this case can be attributed to the low degree of covalence between the ligand atoms and the Eu center, as well as to the high symmetry of the central site. The high value of Ω_4 can be explained with basis on the interactions between the neighborhood units, as shown in the crystal structure. Table 3 shows some complexes and their intensity parameters Ω_2 and Ω_4 [29–31]. It is possible to observe that ligands like β-diketones show a high value of Ω_2 because of the highly polarizability environment. On the other hand, the complexes with acid groups as ligands normally show a low value of Ω_2 due to the more accentuated ionic character of the metal–ligand bond. The europium complex **1** belongs to the class of the more ionic complexes due to the low covalent character between nitrogen/oxygen atoms and the europium ion.

The ground state geometry of [Eu(dfpbpsc–H^+)$_2$]NO_3 (**1**) was calculated using Sparkle/AM1 [16] implemented in MOPAC2009 package [17] and is shown in Fig. 10, compared with the structure obtained through X-ray monocrystal diffractometry. We can observe that the structure obtained from Sparkle/AM1 shows some

Table 3
Some comparative Ω_2 and Ω_4 intensity parameters.

Complex	$\Omega_2/10^{-20}$ cm^2	$\Omega_4/10^{-20}$ cm^2	References
[Eu(tta)$_3$(H$_2$O)$_2$]	33	4.6	[28]
[Eu(absecl)$_3$(H$_2$O)$_2$]	8.8	5.6	[29]
[Eu(abse)$_3$(H$_2$O)$_2$](H$_2$O)$_2$	6.4	6.0	[29]
[Eu(dpa)$_3$]$^{3-}$	6.1	3.5	[30]
[Eu(donic)$_3$]$^{3-}$	6.3	3.4	[30]

tta: theoyltrifluoroacetonate; absecl: 4-chloro-benzeneseleninic acid; abse: benzeneseleninic acid; dpa: pyridine-2,6-dicarboxylic acid; donic: quelidonic acid.

Table 2
Intensity parameters, radiative, non-radiative and total emission rates, emission lifetime of the $^5D_0$ state and quantum efficiency for complex **1**.

$\Omega_2/10^{-20}$ cm^2	$\Omega_4/10^{-20}$ cm^2	R_{02}	A_{rad}/s^{-1}	A_{nrad}/s^{-1}	A_{tot}/s^{-1}	τ/ms	η/%
5.5	7.2	0.021	254	49 672	50 000	0.02	0.51

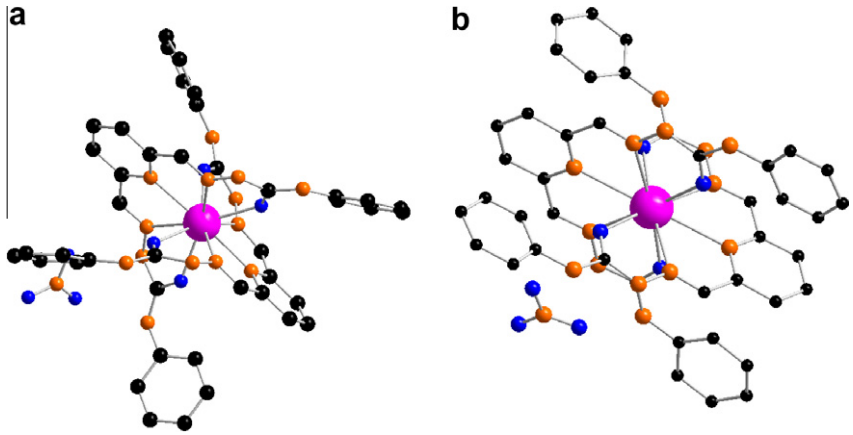

Fig. 10. Structure of the cation $[Eu(dfpbpsc–H^+)_2]^+$ (**1**). (a) Provided by Sparkle/AM1. (b) Provided by monocrystal X-ray diffraction.

Table 4
Polar coordinates for $[Eu(dfpbpsc–H^+)_2]NO_3$ (**1**) from Sparkle/AM1. In parenthesis are shown the values provided by X-ray diffractometry data.

Bond	d (Å)	θ (°)	Φ (°)
Eu–O(A)	2.4447 (2.4084)	161.1807 (157.2467)	306.4921 (234.5696)
Eu–N(A)	2.5787 (2.6666)	137.7885 (92.9234)	92.4479 (184.9977)
Eu–N(B)	2.5459 (2.7849)	85.7878 (84.4571)	132.7655 (61.3269)
Eu–N(C)	2.5820 (2.6882)	39.3016 (91.2789)	183.7162 (300.9455)
Eu–O(B)	2.4325 (2.4421)	31.3227 (32.6581)	298.5309 (239.2898)
Eu–O(A)	2.4283 (2.4420)	68.8032 (90.0000)	66.9343 (0.0000)
Eu–N(A)	2.5846 (2.6865)	91.7294 (26.4174)	11.4535 (57.8523)
Eu–N(B)	2.5446 (2.7856)	96.0003 (94.0348)	308.3734 (242.8724)
Eu–N(C)	2.5725 (2.6664)	89.1536 (142.2037)	245.7367 (63.7015)
Eu–O(B)	2.4509 (2.4072)	115.2636 (90.0000)	192.0045 (124.6605)

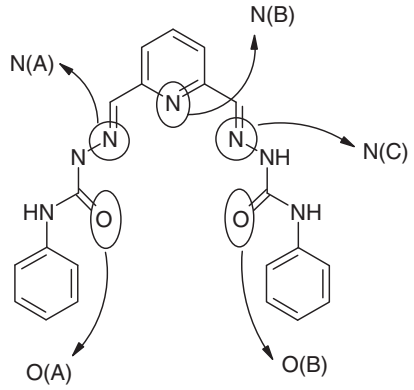

Fig. 11. Codes proposed for nitrogen and oxygen atoms.

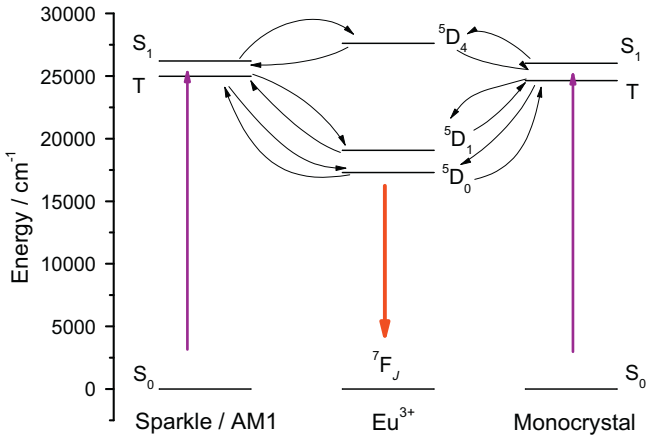

Fig. 13. Energy level diagram, with the ligands levels calculated from Sparkle/AM1 (left side) and X-ray monocrystal data (right side).

differences if compared with the single-crystal structure. The aromatic rings in the Sparkle/AM1 drawing are not in the same plane, probably because of the high repulsion between the aromatic and pyridine rings. The polar coordinates are shown in Table 4. To differentiate the oxygen and nitrogen atoms in Table 4 we propose the codes shown in Fig. 11. The average Eu–O/Eu–N distances calculated from Sparkle/AM1 are respectively 2.4391 and 2.5681 Å. The average distances for these two parameters, obtained from X-ray monocrystal analysis, are 2.4246 and 2.7130 Å, correspondingly. The Sparkle/AM1 error for the Eu–O distance is 0.60%, and for the Eu–N distance is somewhat bigger, 5.3%.

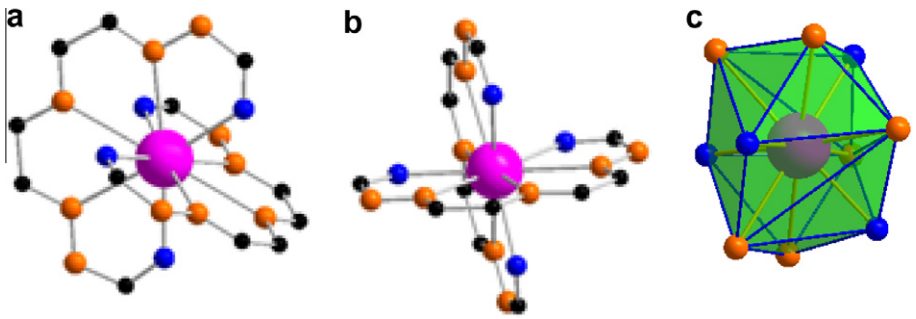

Fig. 12. Coordination polyhedron of $[Eu(dfpbpsc–H^+)_2]^+$ (**1**). In (a) and (b) are shown two different views of the complex, without hydrogen atoms. (c) Local polyhedron of the europium ion.

Table 5
Transfer and back transfer rates calculated from Sparkle/AM1 data and X-ray monocrystal data.

	$S_1 \rightarrow {}^5D_4/s^{-1}$	${}^5D_4 \rightarrow S_1/s^{-1}$	$T \rightarrow {}^5D_1/s^{-1}$	${}^5D_1 \rightarrow T/s^{-1}$	$T \rightarrow {}^5D_0/s^{-1}$	${}^5D_0 \rightarrow T/s^{-1}$
Sparkle/AM1	2.1×10^7	1.6×10^{10}	2.9×10^9	1.7×10^{-3}	5.9×10^8	7.4×10^{-8}
Monocrystal	6.5×10^6	1.2×10^{10}	5.1×10^9	1.5×10^{-2}	1.1×10^9	7.3×10^{-7}

Table 6
Population of the ligand levels (S_0, S_1 and T) and europium levels (${}^5D_4$, ${}^5D_1$ and ${}^5D_0$).

	S_0	S_1	T	${}^5D_4$	${}^5D_1$	${}^5D_0$
Sparkle/AM1	0.83	8.2×10^{-5}	2.3×10^{-6}	1.1×10^{-7}	6.8×10^{-3}	0.16
Monocrystal	0.83	8.2×10^{-5}	1.3×10^{-6}	4.3×10^{-8}	6.7×10^{-3}	0.16

The coordination polyhedron of the europium ion obtained from Sparkle/AM1 with the X-ray crystallographic data is shown in Fig. 12. It is possible to observe a highly symmetric site around the europium center, with the coordination number 10, and the point symmetry near a C_{2v} group.

3.6. Transfer rates

In a lanthanide complex the ligand has the function of absorbing energy in the UV region and transfer it to the lanthanide ion. The most important transferences are those between S_1 (excited singlet) and ${}^5D_4$, T (triplet) and ${}^5D_1$, and T and ${}^5D_0$. Some methods developed by Malta and co-workers allow determining the energy transfer between ligand and metal [32–34]. Fig. 13 shows the scheme of energy levels of the ligand (obtained from Sparkle/AM1 and crystallographic data) and energy levels of the europium ion. The transfer and back transfer rates are shown as well. Table 5 shows the calculated transfer and back transfer rates. There is a large back transfer rate between S_1 and ${}^5D_4$, contributing to decrease the emission of the europium ion. However, there are large transfer rates between T and ${}^5D_1$ and ${}^5D_0$.

The population of the energy levels of the ligand/europium ion was calculated using the adequate kinetic equations described in the literature [35]. The calculated populations, resumed in Table 6, show a very high density in the S_0 level and a low density in the ${}^5D_0$ emission level of the europium ion. These different values of populations can be attributed to the resonance between N–H and C–H vibrations, coupled with the emission level of europium, promoting a quenching in the luminescence and the non-radiative processes in the ligand molecule, regardless of the emission of the ligand.

The theoretical quantum yield was calculated according to the following equation [35]:

$$q_{\mathrm{THEO}} = \frac{A_{rad} N({}^5D_0)}{\phi_0 N(S_0)}$$

where A_{rad} is the radiative emission rate, $N({}^5D_0)$ is the steady-state population, Φ_0 is the absorption rate from the ligand singlet ground-state S_0, with steady-state population $N(S_0)$, to the singlet ligand excited state S_1. It was found a theoretical quantum yield of 0.50%, using the X-ray monocrystal data and Sparkle/AM1 data. The theoretical quantum yield is in very good agreement with the quantum efficiency calculated with the experimental data, showing that the emission through the ${}^5D_0$ level of Eu^{3+} is the main channel.

4. Conclusions

The new synthesized complexes **1**, **2** and **3** show coordination numbers which can not be considered uncommon, for lanthanide chelates. In the case of complex **1**, the low covalence degree of the coordinative ligand–europium bonds could be also calculated. It was also shown that the ground state geometry calculated from Sparkle/AM1 is in good agreement with the geometry obtained from X-ray monocrystal data. The theoretical calculations are valuable instruments for understanding the occurrence of several experimental data and can be helpful to design new complexes according to specific properties or interests.

Acknowledgments

This work was supported with funds from CAPES, CNPq, FAPESP and FAPERGS (Brazilian agencies). We are very grateful to Prof. A.M. Simas (CCEN-UFPE) by transferring the Sparkle/AM1 knowledge and by the help with the computational techniques. We are also very grateful to Prof. O.L. Malta (CCEN-UFPE) by transferring the knowledge about the 4f–4f intensities theory and by the interpretation of the Judd-Ofelt [36,37] intensity parameters.

Appendix A. Supplementary data

CCDC 794124, 794125 and 794126 contains the supplementary crystallographic data for **1**, **2** and **3**. These data can be obtained free of charge via http://www.ccdc.cam.ac.uk/conts/retrieving.html, or from the Cambridge Crystallographic Data Centre, 12 Union Road, Cambridge CB2 1EZ, UK; fax: (+44) 1223-336-033; or e-mail: deposit@ccdc.cam.ac.uk.

References

[1] G.R. Choppin, D.R. Peterman, Coord. Chem. Rev. 174 (1998) 283.
[2] G. Manzoni de Oliveira, M. Hörner, A. Machado, D.F. Back, J.H.S.K. Monteiro, M.R. Davolos, Inorg. Chim. Acta, doi:10.1016/j.ica.2010.11.007.
[3] J.M. Lehn, Angew. Chem., Int. Ed. Engl. 29 (1990) 1304.
[4] D. Parker, J.A.G. Williams, J. Chem. Soc., Dalton Trans. (1996) 3613.
[5] T.R. Cundari, M.T. Benson, L.C. Saunders, S.O. Sommerer, Inorg. Chim. Acta 258 (1997) 127.
[6] M. Gaye, F.B. Tamboura, M. Dyop, A.S. Sall, A.H. Barry, T. Jouini, Inorg. Chem. Commun. 6 (2003) 1004.
[7] U. Abram, A. Jagst, A. Sanchez, E.M. Vázquez-López, Inorg. Chem. 44 (2005) 5738.
[8] Alexander Jagst, Polydentate Hydrazone Ligands for Complexation of Metal Ions with Relevance in the Nuclear Medicine, Ph.D. Thesis, Institut für Biologie, Chemie und Pharmazie, Freie Universität, Berlin, 2007.
[9] K. Binnemans, Chem. Rev. 109 (2009) 4274.
[10] G. Gasparotto, M.A. Cebim, M.S. Goes, S.A.M. Lima, M.R. Davolos, J.A. Varela, C.O. Paiva-Santos, M.A. Zaghete, J. Appl. Phys. 106 (2009) 063509.
[11] E.G. Moore, A.P.S. Samuel, K.N. Raymond, Acc. Chem. Res. 42 (2009) 542.
[12] J. Kido, Y. Okamoto, Chem. Rev. 102 (2002) 2357.
[13] W.G. Quirino, R.D. Adati, S.A.M. Lima, C. Legnani, M. Jafelicci Jr., M.R. Davolos, M. Cremona, Thin Solid Films 515 (2006) 927.
[14] A.V.M. Andrade, N.B. Costa, A.M. Simas, G.F. Sá, Chem. Phys. Lett. 227 (1994) 349.
[15] G.M. Sheldrick, Acta Crystallogr., Sect. A 64 (2008) 112.
[16] R.O. Freire, G.B. Rocha, A.M. Simas, Inorg. Chem. 44 (2005) 3299.

[17] J.J.P. Stewart, MOPAC 2009 Manual, Colorado Springs, Stewart Computational Chemistry, 2009.
[18] M.O. Rodrigues, N.B. Costa Júnior, C.A. Simone, A.A.S. Araújo, A.M. Brito-Silva, F.A.A. Paz, M.E. Mesquita, S. Alves Jr., R.O. Freire, J. Phys. Chem. B 112 (2008) 4204.
[19] E.R. Santos, M.A.C. Santos, R.O. Freire, S. Alves Jr., L.S. Barreto, M.E. Mesquita, Chem. Phys. Lett. 418 (2006) 337.
[20] A.P. Souza, F.A.A. Paz, R.O. Freire, L.D. Carlos, O.L. Malta, S. Alves Jr., G.F. Sá, J. Phys. Chem. B 111 (2007) 9228.
[21] J.E. Ridley, M.C. Zerner, Theor. Chim. Acta 42 (1976) 223.
[22] M.C. Zerner, G.H. Loew, R.F. Kirchner, U.T. Mueller-Westerhoff, J. Am. Chem. Soc. 102 (1980) 589.
[23] M.C. Zerner, ZINDO Manual: Quantum Theory Project, University of Florida, Gainesville, 1990.
[24] A. Ruiz-Martínez, S. Alvarez, Chem. Eur. J. 15 (2009) 7470.
[25] D.L. Pavia, G.M. Lampman, G.S. Kriz, Introduction to Spectroscopy: a Guide for Students of Organic Chemistry, third ed., Thomson Learning, South Melbourne, 2001. p. 579.
[26] G.B. Rocha, R.O. Freire, A.M. Simas, J.J.P. Stewart, J. Comput. Chem. 27 (2006) 1101.
[27] R.A. Sá Ferreira, S.S. Nobre, C.M. Granadeiro, H.I.S. Nogueira, L.D. Carlos, O.L. Malta, J. Lumin. 121 (2006) 561.
[28] W.T. Carnall, H. Crosswhite, H.M. Crosswhite, Energy Structure and Transition Probabilities of the Trivalent Lanthanides in LaF_3, Argonne National Laboratory Report, unnumbered, 1977.
[29] O.L. Malta, H.F. Brito, J.F.S. Menezes, F.R. Gonçalves e Silva, S. Alves Jr., F.S. Farias Jr., A.V.M. Andrade, J. Lumin. 75 (1997) 255.
[30] A.P. Souza, L.C.V. Rodrigues, H.F. Brito, S. Alves Jr., O.L. Malta, J. Lumin. 130 (2010) 181.
[31] P.P. Lima, O.L. Malta, S. Alves Jr., Quím. Nova 28 (2005) 805.
[32] O.L. Malta, J. Lumin. 71 (1997) 229.
[33] F.R.G.E. Silva, O.L. Malta, J. Alloys Compd. 250 (1997) 427.
[34] O.L. Malta, J. Non-Cryst. Solids 354 (2008) 4770.
[35] G.F. Sá, O.L. Malta, C.M. Donegá, A.M. Simas, R.L. Longo, P.A. Santa-Cruz, E.F. Silva Jr., Coord. Chem. Rev. 196 (2000) 165.
[36] B.R. Judd, Phys. Rev. 127 (1962) 750.
[37] G.S. Ofelt, J. Chem. Phys. 37 (1962) 511.